Research Article

Received: 7 June 2022 Revised: 7 September 2022 Accepted article published: 18 September 2022 Published online in Wiley Online Library: 5 October 2022

(wileyonlinelibrary.com) DOI 10.1002/jctb.7235

Removal of amoxicillin and ampicillin using manganese dioxide/montmorillonite composite

Vera Valovicova,[a] Eva Plevova,[a*] Silvie Vallova,[b,c] Lenka Vaculikova,[a] Aneta Smykalova,[b,c] Bogna D Napruszewska,[d] Ewa M Serwicka[d] and Silvia Dolinska[e]

Abstract

BACKGROUND: Clay-based materials represent great potential for the development of efficient and environmentally friendly sorbents. The study focuses on a laboratory-obtained manganese dioxide/montmorillonite (MnO_2/MMT) composite for removal of two types of antibiotics – amoxicillin (AMX) and ampicillin (AMP) – from aqueous solution.

RESULTS: The composite was successfully prepared using a reduction procedure involving the reaction between potassium permanganate ($KMnO_4$) and hydrochloric acid (HCl) to form MnO_2 followed by the addition of MMT. X-ray analysis, scanning electron microscopy, X-ray fluorescence and Fourier transform infrared spectroscopy were performed for characterization of physicochemical and structural properties, simultaneous thermogravimetry and differential scanning calorimetry for estimation of thermal stability and high-performance liquid chromatography for determination of antibiotic equilibrium concentrations in aqueous solution. The precipitated MnO_2 component, manifested by long fibers, corresponded to the tunnel structure of cryptomelane. In the case of MnO_2/MMT it is evident that MnO_2 developed short fibers with the participation of the MMT matrix. The thermal data suggested that the MnO_2 phase upon contact with the clay support showed better thermal stability. The final decomposition of Mn_2O_3 was shifted to higher temperature of 985 °C. Adsorption procedure in a batch regimen showed sufficient sorption ability for both antibiotics with over 90% efficiency. For AMP the value of q_{max} was about 45 mg g^{-1} and for AMX it was only 21 mg g^{-1}.

CONCLUSIONS: The results provided valuable information for the design of a potentially inexpensive clay-based adsorbent and demonstrated the removal of two types of broad-spectrum β-lactam antibiotics from aqueous solution to a sufficient degree.

Keywords: montmorillonite; MnO_2; composite; sorption; amoxicillin; ampicillin

INTRODUCTION

Pharmaceutical consumption has been rapidly increasing in recent years. Among the most used drugs in human medicine are analgesics, anti-inflammatory drugs, contraceptives, beta-blockers, neuroactive pharmaceuticals and mainly antibiotics. Unfortunately, these substances cannot be effectively removed by wastewater treatment and their biodegradability is very low. Drugs have been detected in the whole environment with various concentrations, from nanogram to milligram levels.[1,2] Although these concentrations do not appear to be alarming, such substances have a long-lasting and detrimental effect not only on the environment, but also on human and animal health. Therefore, the development of effective technologies for adsorption of drugs from wastewater is very important.[3-5]

Probably the longest known and most widely used material for the uptake of organic contaminants from water resources is granular activated carbon. Using these types of sorbents, however, carries certain limits connected to high costs or difficult sorbent regeneration processes. Moreover, the capacity of granular activated carbon may decrease drastically in the next few years relating to the continuing declining production of coal worldwide.[6-8] Therefore, other potentially cheaper adsorbents for the adsorption of organic contaminants are currently being

* Correspondence to: E Plevova, Institute of Geonics of the Czech Academy Sciences, Studentska 1768, 708 00 Ostrava-Poruba, Czech Republic, E-mail: eva.plevova@ugn.cas.cz

a Institute of Geonics of the Czech Academy Sciences, Ostrava-Poruba, Czech Republic

b Institute of Environmental Technology CEET, VSB-Technical University of Ostrava, Ostrava-Poruba, Czech Republic

c Department of Chemistry, VSB-Technical University of Ostrava, Ostrava-Poruba, Czech Republic

d Jerzy Haber Institute of Catalysis and Surface Chemistry, Polish Academy of Sciences, Krakow, Poland

e Institute of Geotechnics of the Slovak Academy of Sciences, Kosice, Slovak Republic

investigated. Composite materials based on clay minerals represent a significant development trend in the field of advanced materials with predefined properties, designed for various applications in sorption processes.[9-12]

Montmorillonite, a phyllosilicate with a 2:1 structure, has become one of the most widely used clay minerals for the preparation of composites.[9,13,14] The clay mineral matrix of such composites serves as basis for modification/intercalation of organic by inorganic substances. Generally, the modification process is based on replacing the interlayer cations by organo-cations like alkylammonium or alkylphosphonium cations. Such ion exchange modifies the hydrophilic disposition to organophilic, which enables intercalation and sorption of the organic compounds like polyaromatic hydrocarbons, pharmaceuticals, pesticides, tenzides, etc.[15-20] But using organic compounds like alkylammonium or alkylphosphonium cations can bring some limitations like quite high cost, lower accessibility or potential gradual desorption of alkylammonium and alkylphosphonium cations leading to the reduction of the adsorption capacity of the prepared organoclay composite and also such released surfactant can become a further potential pollutant in the environment.[21,22] Using low-cost and low-toxicity oxides for the preparation of inorganic clay composites seems to be one of the directions for obtaining composites with high sorption capacity and eliminating problems with surfactants described above. Among suitable inorganic compounds are active phases based on MnO_x, Fe_xO_y, etc.[23-26]

Therefore, the work reported here aimed at the synthesis of a composite based on montmorillonite and MnO_2 for the purpose of evaluating its thermal stability and effectiveness in adsorbing two types of commonly used antibiotics from aqueous solutions. The uniqueness of the research lies in the design and preparation of a potentially low-cost sorbent based on clay mineral for the adsorption with sufficient efficiency of relatively new and alarming pollutants like drugs and other pharmaceutical products.

SAMPLES AND METHODS

Ca-rich montmorillonite STx-1b (MMT) from Texas (USA) obtained from the Clay Minerals Society was used for the design and preparation of the MnO_2/MMT composite. All laboratory experiments were performed with a 5 μm fine-grained fraction. The fundamental physicochemical properties of this MMT have been described in detail previously.[27-29] $KMnO_4$ and HCl of analytical purity were used for composite preparation and were purchased from Merck Ltd, Germany. For adsorption procedures, amoxicillin (AMX) and ampicillin (AMP) with molecular weights of 365.4 and 349.4 g mol^{-1} were chosen and both were supplied by Sigma Aldrich USA. The MnO_2/MMT composite was prepared using a reductive procedure.[30,31] The procedure was utilized to precipitate colloids of manganese oxides onto MMT in a weight ratio of 1:1. A control reference MnO_2 sample was prepared in the same manner as the composite, but without MMT.

Solid manganese oxides were formed in solution via the reaction

$$2KMnO_4 + 8HCl \rightarrow 2MnO_2 + 2KCl + 3Cl_2 + 4H_2O \quad (1)$$

The procedure involved 27.26 g of $KMnO_4$, dissolved in 30 mL of deionized water, being heated at 90 °C. An amount of 15 g of MMT was added gradually and the resulting suspension was further stirred for 10 min with HCl dropwise addition. After stirring and heating in a water bath for an additional 25 min, the suspension was filtered and washed several times using deionized water. The final product was dried at 95 °C for 24 h and ground to a fine powder for experimental use.

X-ray fluorescence analysis

The determination of major elements was performed by means of a wavelength-dispersive sequential X-ray fluorescence spectrometer (ARL PERFORM'X 4200 W, Thermo Scientific, USA). The fusion bead method was preferred for the preparation of pressed pellets in order to eliminate the heterogeneity due to grain size and a mineralogical effect and to reduce inter-element effects by dilution of the sample. Fused beads (40 mm) were prepared by fusion of the samples with lithium tetraborate using a VULCAN 4M fusion machine in Pt/Au crucibles.

Powder X-ray diffraction (XRD)

Measurements were carried out with the use of a Panalytical X'Pert Pro powder diffractometer in the 2θ range 5–65° range with a 0.0334° step size. The following parameters were used: Cu Kα radiation at 40 kV and 30 mA, 10 mm constant irradiated length of sample obtained by the use of an automatic programmed divergence slit, primary and secondary Soller slits, flat graphite monochromator of secondary beam and multiposition X'Celerator detector.

Scanning electron microscopy (SEM)

Sample morphology was investigated using a JSM-7500F field emission SEM instrument (JEOL, Japan) a voltage of acceleration of 20 kV and magnification of ×20 000.

Fourier transform infrared (FTIR) spectroscopy

FTIR spectra were acquired using a Nicolet 6700 FTIR spectrometer (ThermoScientific) equipped with DTGS/KBr. The KBr pressed-disc technique was used for routine scanning of the spectra. Approximately 1 mg of powder sample was mixed with 200 mg of dried KBr to make a good-quality KBr pellet. For each sample, 64 scans in the spectral range 400–4000 cm^{-1} were measured with a resolution of 4 cm^{-1}.

Simultaneous thermogravimetry and differential scanning calorimetry (TG/DSC)

TG/DSC curves were obtained with simultaneous TG/DSC apparatus (TA Instruments SDT 650). TG/DSC curves were recorded under the following conditions: sample mass, about 10 mg; final temperature, 1000 °C; heating rate, 10 °C min^{-1}; dry air flow rate, about 100 cm^3 min^{-1}; reference material, Al_2O_3; no pressing in crucible.

High performance liquid chromatography (HPLC)

The amounts of AMX and AMP were determined using HPLC (Waters 2996, Waters Corporation, Milford). A Synergi 4 μm Polar-RP 80 Å column was used, with mobile phase of water solution and methanol solution at a flow of 0.5 mL min^{-1}.

Sorption experiments

Sorption experiments were performed in a batch regimen with 100 mg of sorbent, 20 mL of each antibiotic solution with initial concentrations ranging from 10 to 100 mg L^{-1}. The suspension of sorbent with solution of antibiotics was mixed on a rotary tumbler for 24 h at room temperature, then it was centrifuged and filtered. The equilibrium concentration of AMX and AMP in solution was determined using HPLC.

The amount of antibiotics at equilibrium was obtained using the following equation[32]:

$$q_e = \frac{(c_0 - c_e)V}{m} \quad (1)$$

where q_e is the amount of antibiotic per unit of sorbent (mg g^{-1}), c_0 is the initial concentration of antibiotic in solution (mg L^{-1}), c_e is the equilibrium concentration of antibiotic in solution (mg L^{-1}), m is the mass of sorbent (g) and V is the volume of solution (L).

Isotherm parameters were determined using the Freundlich/Langmuir equations.[33] Freundlich:

$$\ln q_e = \ln K_F + \frac{\ln c_e}{n} \quad (2)$$

Langmuir:

$$\frac{c_e}{q_e} = \frac{1}{q_{max} K_L} + \frac{c_e}{q_{max}} \quad (3)$$

where c_e is the equilibrium concentration of antibiotics in solution (mg L^{-1}), q_e is the equilibrium adsorption capacity of antibiotics per unit of sorbent (mg g^{-1}), q_{max} is the maximal sorption capacity of antibiotics per unit of sorbent (mg g^{-1}), K_F and n are Freundlich constants related to the adsorption capacity and adsorption strength and K_L is the Langmuir constant corresponding to the free energy of adsorption.

RESULTS AND DISCUSSION

X-ray fluorescence analysis

The elemental composition (expressed in oxides) of MMT samples is summarized in Table 1.

XRD analysis

The XRD analysis of MMT indicated a typical MMT mineral with interlayer spacing value $d_{001} = 1.49$ nm. XRD patterns of MnO_2 (Fig. 1) showed that the preparation process led to the formation of manganese oxide of cryptomelane type, α-phase (ref. 00-042-1348). A reflection at $2\theta = 42.5°$ showed the presence of ε-phase admixture (ref. 04-005-4883). The XRD pattern of

Table 1. Content (%) of major elements

Sample	CaO	SiO_2	Al_2O_3	MgO	Fe_2O_3	K_2O	TiO_2	Na_2O
MMT	1.7	65.3	12.6	2.7	0.9	0.2	0.1	0.2

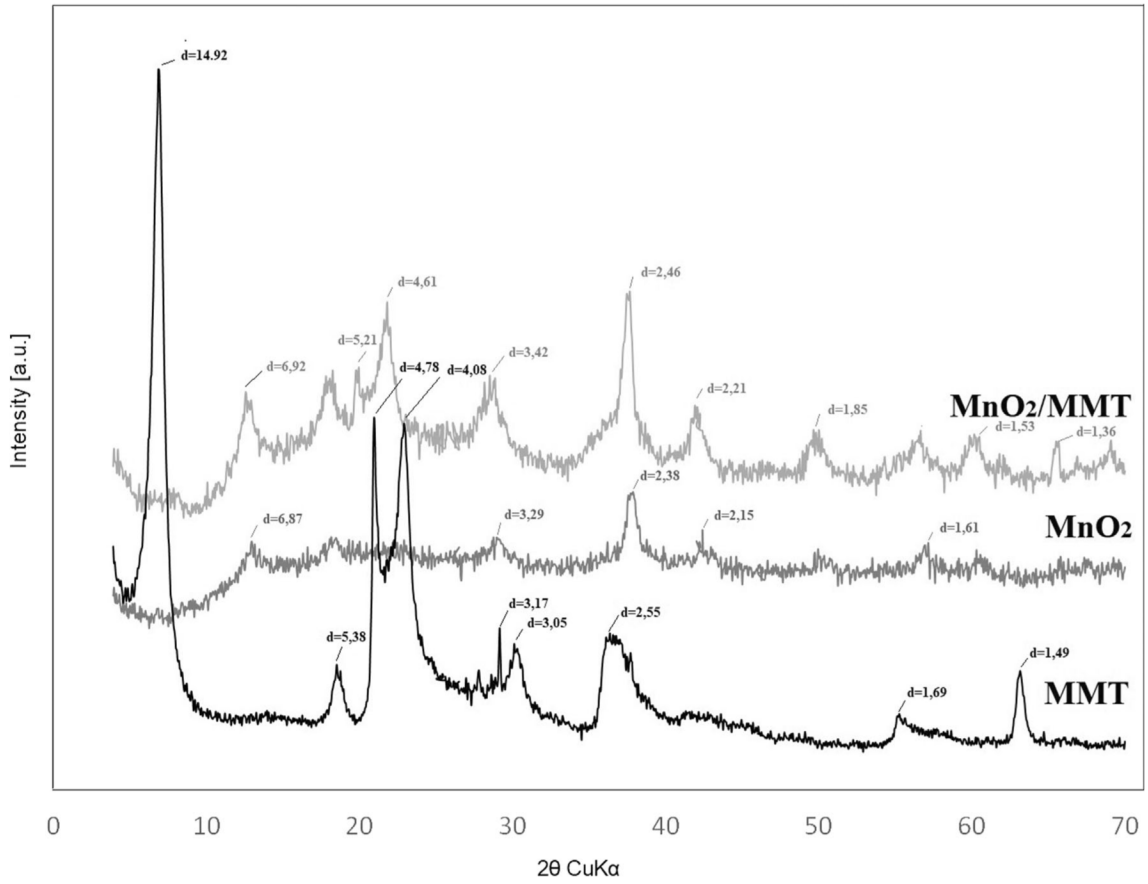

Figure 1. XRD patterns of MMT, MnO_2 and MnO_2/MMT.

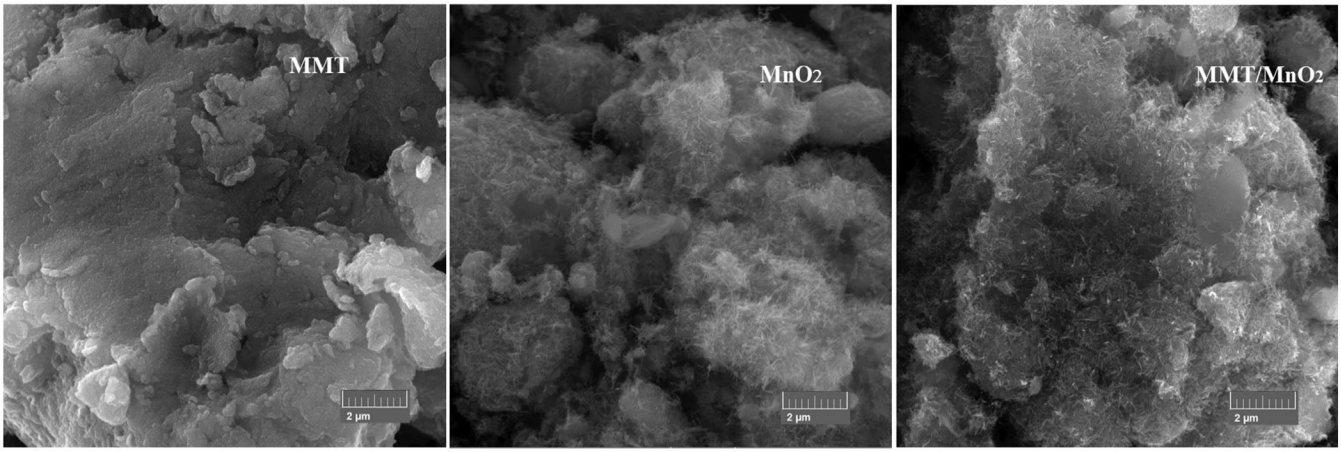

Figure 2. SEM images of MMT, MnO_2 and MnO_2/MMT.

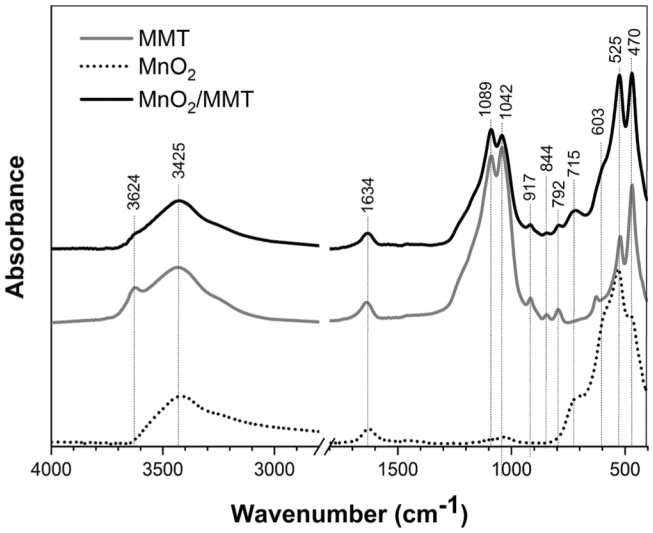

Figure 3. FTIR spectra of MMT, MnO_2 and MnO_2/MMT.

MMT/MnO_2 recorded the reflection of both the clay component and the cryptomelane component, although the lower intensity d_{001} for MMT indicated the absence of the order of layer stacking. Small amounts of quartz and opal impurities were also detected in the composite sample.

SEM analysis

SEM images of samples were obtained at ×20 000 magnification. MMT is characterized by particles assembled into massive flake aggregates. MnO_2 sample forms fiber spherical agglomerates up to 80 nm long and 3 nm wide. In the case of MnO_2/MMT, morphology showed that manganese oxides precipitated on the clay in the form of fibers which are typical for cryptomelane, but are shorter than in case of the reference MnO_2 (Fig. 2). The trend in morphology is similar to SEM results reported previously.[34]

Infrared spectroscopy

The positions of the characteristic MMT absorption bands remained almost unchanged for the MnO_2/MMT sample, proving that the formation of the clay composite did not cause structural

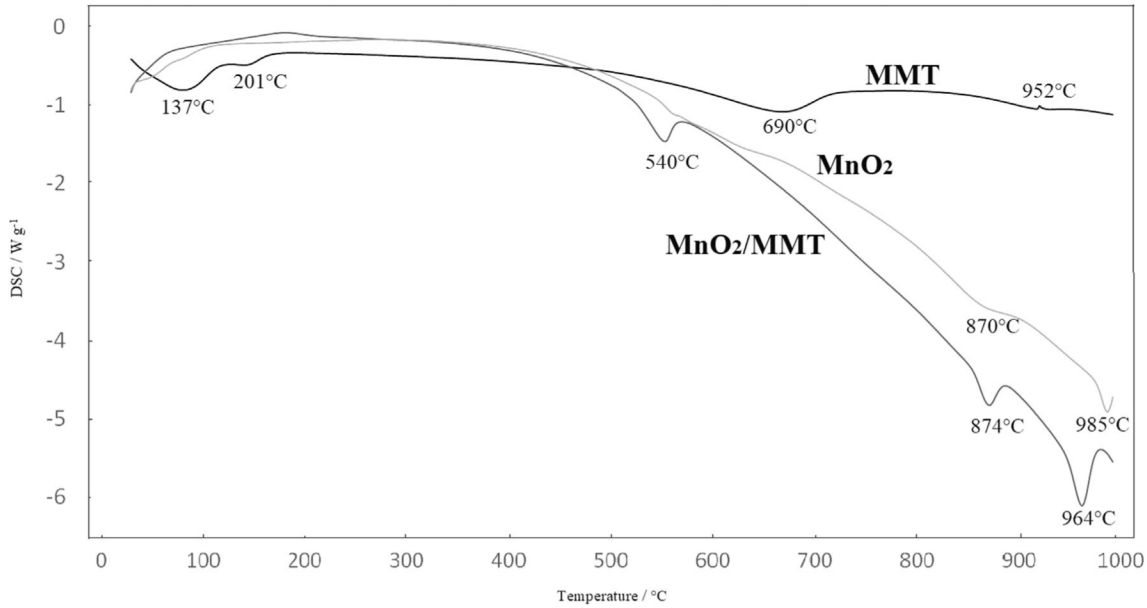

Figure 4. DSC curves of MMT, MnO_2 and MnO_2/MMT.

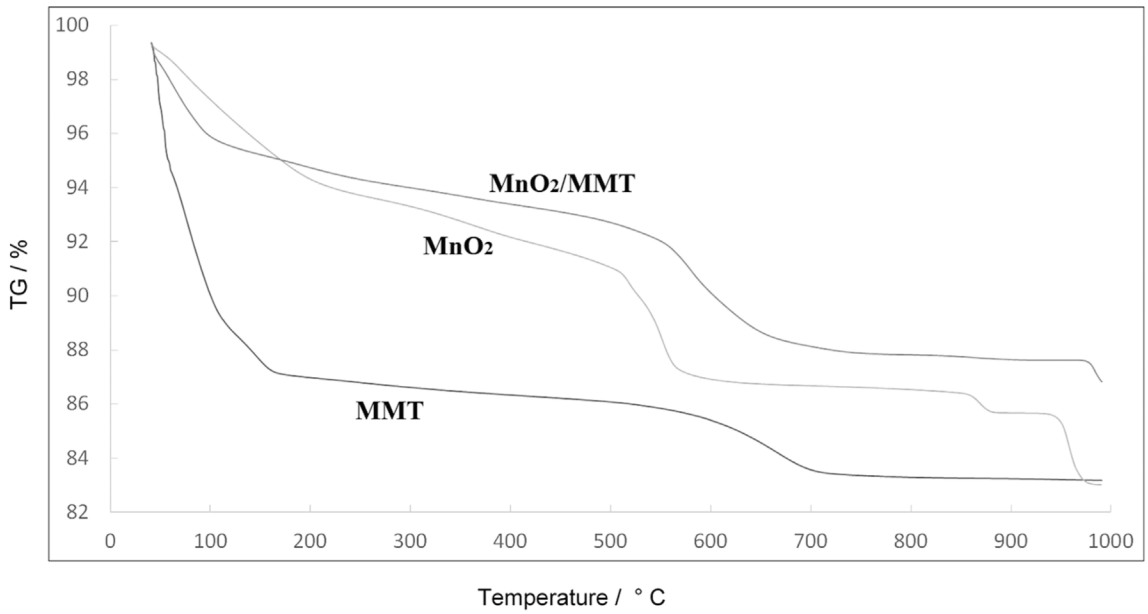

Figure 5. TG curves of MMT, MnO_2 and MnO_2/MMT.

changes in the original clay mineral (Fig. 3). Modification with inorganic cations significantly affected only the bands associated with the stretching vibrations of the OH groups at 3624 cm^{-1} and the deformation vibrations lying at 917 cm^{-1}, both bands showing a lower intensity. This fact may be related to changes in the layer stacking order of the clay mineral during composite formation. A more detailed spectral study of STx-1b MMT is described elsewhere.[35,36]

The presence of MnO_2 phase in the laboratory-prepared MnO_2/MMT composite is evidenced by the weak bands at 715 and 603 cm^{-1} together with the sharp band lying at 525 cm^{-1}, which overlaps with the Al-Si-O deformation vibrations of MMT. These spectral bands are closely related to vibrations of MnO_6 octahedral framework in the cryptomelane structure,[37] which was also confirmed by XRD analysis.

TG and DSC measurements

Thermal behavior and stability of MMT, MnO_2 and MnO_2/MMT were investigated by simultaneous TG/DSC up to 1000 °C. DSC curves are presented in Fig. 4. TG curves are presented in Fig. 5. Peak temperatures for MMT obtained from the DSC curve are: 137 and 201 °C for dehydration (peak at 201 °C indicates the presence of Ca cations), 690 °C for dehydroxylation and 952 °C for recrystallization/transformation.

Thermal decomposition of MnO_2 sample occurs in three major weight loss stages: up to 200 °C related to the loss of adsorbed water; in the range 200–550 °C, associated with the departure of chemisorbed water and a gradual loss of lattice oxygen leading eventually to the formation of Mn_2O_3 at 540 °C; and in the range 550–1000 °C, attributed to the loss of oxygen accompanying decomposition of Mn_2O_3 to Mn_3O_4.[38] The latter stage is composed of two steps, indicating the presence of two Mn_2O_3 components of different thermal stabilities. XRD analysis showed that MnO_2 sample contains, in addition to cryptomelane, a small admixture of ε-MnO_2. Therefore, the small weight loss connected to the peak at 874 °C corresponds to the decomposition of Mn_2O_3 derived from ε-MnO_2, while the major weight loss related to the peak at 964 °C is due to the final

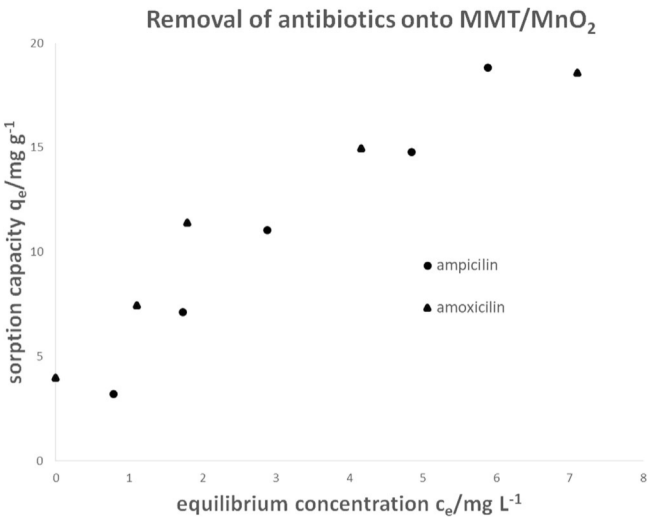

Figure 6. Sorption of AMX and AMP onto MnO_2/MMT.

decomposition of Mn_2O_3 originating from cryptomelane.[39] The corresponding DSC data show that all steps are, as expected, endothermic.

The TG profile of MnO_2/MMT differs from that of MnO_2 sample, because, essentially, only two steps are visible, although the peak is very weak. The first one may be connected to the loss of adsorbed water, while the other most likely reflects the decomposition of the α-MnO_2 component to Mn_2O_3, overlapping with dehydroxylation of clay. At higher temperature the mass loss is only very small (Fig. 5), indicating that most of the Mn_2O_3 intermediate retains its identity, which agrees with XRD analysis showing the presence of Mn_2O_3, and not Mn_3O_4. The peak related to final decomposition of Mn_2O_3 is shifted to higher temperature (985 °C). So, the data point to the stabilization of the manganese oxide phase against thermal decomposition, when in contact with the clay support.

Table 2. Isotherm parameters for adsorption of AMP and AMX onto MnO_2/MMT

	Langmuir			Freundlich		
	R^2	q_{max} (mg g^{-1})	K_L (L mg^{-1})	R^2	K_F ($mg^{-1-1/n}$ $L^{1/n}$ g^{-1})	n
MMT/MnO_2 + AMP	0.941	45.81	0.12	0.992	4.84	1.31
MMT/MnO_2 + AMX	0.941	21.41	0.92	0.976	8.80	2.62

AMX and AMP sorption procedure

The amounts of AMP and AMX adsorbed onto MMT/MnO_2 at equilibrium were determined from the difference between added amount and remaining amount of antibiotics after equilibration according to Eqn (1). The equilibrium antibiotic concentrations were obtained using HPLC. The relation between q_e and c_e obtained for AMP and AMX adsorbed onto MMT/MnO_2 is presented in Fig. 6.

The capacity of the sorption process increased with increasing initial concentration of antibiotics in solution. The highest sorption capacity is comparable (q_e = 18.82 mg g^{-1} for AMP; q_e = 18.58 mg g^{-1} for AMX). However, the adsorption of AMP and AMX on MMT/MnO_2 proceeds differently, which results from the shape of sorption isotherms (Fig. 6). In the case of AMX, the saturation of the sorbent occurred when the value of the sorption capacity q_e has not changed so much with increasing initial concentration c_0. On the other hand, the sorption isotherm for AMP showed generally an increasing character and the sorption capacity q_e increased with the initial concentration c_0. This fact is also proved by comparison of q_{max} determined by calculation with experimental values of q_e. For AMP the value of q_{max} is about 45 mg g^{-1} and for AMX is only 21 mg g^{-1} (Table 2). Differences in adsorption behavior between AMX and AMP are attributed to differences in Coulomb force and interactions due to the presence of hydroxyl group in the AMX chemical structure.[40]

The relation between the adsorbed amount and the equilibrium concentration in solutions was described using two models: Freundlich and Langmuir (Eqns (2) and (3)). The Langmuir model describes monolayer adsorption with probability of adsorption being the same at all points on the surface and the adsorbed molecules do not interfere with each other. This is particularly suitable for chemisorption processes. The Freundlich isotherm, in contrast to the Langmuir isotherm, is not linear even at low pressures and does not show a limit value of the adsorbed amount at high pressures. This model is based on adsorption on a heterogeneous surface accompanied by sites of different sorption energies. Isotherm parameters of sorption of AMP and AMX onto MMT/MnO_2 for the different isotherm models are presented in Table 1. The values of the correlation coefficient R^2 are higher in the Freundlich model than in the Langmuir model. It is evident that the Freundlich model better describes the adsorption data due to providing linear graphs with higher values of regression coefficients.

CONCLUSIONS

The MnO_2/MMT composite, synthetized using a simple reductive procedure based on potassium permanganate and hydrochloric acid with Ca-rich MMT, was characterized from the point of view of both thermal stability and sorption ability. Characterization using XRD and FTIR analyses showed MnO_2 phase with α-MnO_2 tunnel structure. XRD analysis also proved that MnO_2 also contains a small admixture of ε-MnO_2. According to SEM analysis, α-MnO_2 formed in the presence of a clay component displayed much shorter fibers than the original reference MnO_2 which forms fiber spherical agglomerates up to 80 nm long and 3 nm wide. The thermal decomposition of MMT included three steps such as releasing water layer by layer, releasing constituent water with crystal lattice breaks and recrystallization and transformation. Thermal decomposition of MnO_2 was realized mainly with the formation of Mn_2O_3 followed by decomposition of Mn_2O_3 to Mn_3O_4. Thermal curves of MnO_2/MMT mainly reflect the decomposition of MnO_2 with formation of Mn_2O_3, overlapping with dehydroxylation of clay. The obtained data indicate the stabilization of the manganese oxide phase against thermal decomposition in the case of the contact with clay substance. The sorption capacity of MMT with MnO_2 as a promising sorbent for AMP and AMX was also estimated. Removal of both antibiotics from aqueous solutions showed over 90% efficiency. For AMP the value of q_{max} was about 45 mg g^{-1} and for AMX was only 21 mg g^{-1}. From the results it is evident that the treatment of MMT with MnO_2 leads to the formation of a composite with sufficient sorption capacity for the absorption of AMP and AMX with respect to their relatively low concentrations in wastewater.

ACKNOWLEDGEMENTS

This research was supported from ERDF Institute of Environmental Technology – Excellent Research (no. CZ.02.1.01/0.0/0.0/16_019/0000853). Experimental data were obtained using Large Research Infrastructure ENREGAT supported by the Ministry of Education, Youth and Sports of the Czech Republic under project no. LM2018098. This work was also supported by Mobility programme of the Czech Academy of Sciences and the Slovak Academy of Sciences, Mobility Plus Project, no. SAV-21-08. The authors thank George Layner for checking the English of the manuscript.

REFERENCES

1 Franca DB, Trigueiro P, Silva Filho EC, Fonseca MG and Jaber M, Monitoring diclofenac adsorption by organophilic alkylpyridinium bentonites. *Chemosphere* **242**:125109 (2020).
2 Martucci A, Pasti L, Marchetti N, Cavazzini A, Dondi F and Alberti A, Adsorption of pharmaceuticals from aqueous solutions on synthetic zeolites. *Microporous Mesoporous Mater* **148**:174–183 (2012).
3 Lozano-Morales V, Gardi I, Nir S and Undabeytia T, Removal of pharmaceuticals from water by clay-cationic starch sorbents. *J Cleaner Prod* **190**:703–711 (2018).
4 Davila-Estrada M, Ramirez-Garcia JJ, Solache-Rios MJ and Gallegos-Perez JL, Kinetic and equilibrium sorption studies of ceftriaxone and paracetamol by surfactant-modified zeolite. *Water Air Soil Pollut* **229**:1–9 (2018).
5 Guegan R and Le Forestier L, Performance evaluation of organoclays for the amoxicillin retention in a dynamic context. *Chem Eng J* **406**: 126859 (2021).
6 Zhou W, Meng X, Gao J, Zhao H, Zhao G and Ma J, Electrochemical regeneration of carbon-based adsorbents: a review of regeneration mechanisms, reactors, and future prospects. *Chem Eng J Adv* **5**: 100083 (2021).

7 Marques SC, Marcuzzo JM, Baldan MR, Mestre AS and Carvalho AP, Pharmaceuticals removal by activated carbons: role of morphology on cyclic thermal regeneration. *Chem Eng J* **321**:233–244 (2017).
8 Gupta VK, Nayak A, Bhushan B and Agarwal S, A critical analysis on the efficiency of activated carbons from low-cost precursors for heavy metals remediation. *Crit Rev Environ Sci Technol* **45**:613–668 (2015).
9 Zhu R, Chen Q, Zhou Q, Xi Y, Zhu J and He H, Adsorbents based on montmorillonite for contaminant removal from water: a review. *Appl Clay Sci* **123**:239–258 (2016).
10 Jiang JQ and Zeng Z, Comparison of modified montmorillonite adsorbents part II: the effects of the type of raw clays and modification conditions on the adsorption performance. *Chemosphere* **53**:53–62 (2003).
11 Kleyi PE, Ray SS, Abia ALK, Ubomba-Jaswa E, Wesley-Smith J and Maity A, Preparation and evaluation of quaternary imidazolium-modified montmorillonite for disinfection of drinking water. *Appl Clay Sci* **127**:95–104 (2016).
12 Zhang L and Cao J, Pyrolysis and its mechanism of organomontmorillonite (OMMT) influenced by different functional groups. *J Therm Anal Calorim* **137**:1–10 (2019).
13 Vaculíkova L, Plevova E and Ritz M, Characterization of montmorillonites by infrared and Raman spectroscopy for preparation of polymer-clay nanocomposites. *J Nanosci Nanotechnol* **19**:2775–2781 (2019).
14 Abbas A, Sallam AS, Usman AR and Al-Wabel MI, Organoclay-based nanoparticles from montmorillonite and natural clay deposits: synthesis, characteristics, and application for MTBE removal. *Appl Clay Sci* **142**:21–29 (2017).
15 Vallová S, Plevová E, Smutná K, Sokolová B, Vaculíková L, Valovičová V *et al*., Removal of analgesics from aqueous solutions onto montmorillonite KSF. *J Therm Anal Calorim* **147**:1973–1981 (2021).
16 Zhou CH, Jun LC, Gates WP, Zhu TT and Hua YW, Co-intercalation of organic cations/amide molecules into montmorillonite tunable hydrophobicity and swellability. *Appl Clay Sci* **179**:105157 (2019).
17 De Oliveira T, Boussafir M, Fougère L, Destandau E, Sugahara Y and Guégan R, Use of a clay mineral and its nonionic and cationic organoclay derivatives for the removal of pharmaceuticals from rural wastewater effluents. *Chemosphere* **259**:127480 (2020).
18 Thiebault T, Boussafir M, Le Forestier L, Le Milbeau C, Monnin L and Guegan R, Competitive adsorption of a pool of pharmaceuticals onto a raw clay mineral. *RSC Adv* **6**:65257–65265 (2016).
19 Awad AM, Shaikh SM, Jalab R, Gulied MH, Nasser MS, Benamor A *et al*., Adsorption of organic pollutants by natural and modified clays: a comprehensive review. *Sep Purif Technol* **228**:115719 (2019).
20 Matusik J, Koteja-Kunecka A, Maziarz P and Kunecka A, Styrene removal by surfactant-modified smectite group minerals: efficiency and factors affecting adsorption/desorption. *Chem Eng J* **428**:130848 (2022).
21 Reeve JP and Fallowfield HJ, The toxicity of cationic surfactant HDTMA-Br desorbed from surfactant modified zeolite, towards faecal indicator and environmental microorganisms. *J Hazard Mater* **339**:208–215 (2017).
22 Bautista-Toledo MI, Rivera-Utrilla J, Méndez-Díaz JD, Sánchez-Polo M and Carrasco-Marín F, Removal of the surfactant sodium dodecylbenzene sulfonate from water by process based on adsorption/bioadsorption and biodegradation. *J Colloid Interface Sci* **418**:113–119 (2014).
23 Sohrabi N, Mohammadi R, Ghassemzadeh HR and Heris S, Equilibrium, kinetic and thermodynamic study of diazinon adsorption from water by clay/GO/Fe_3O_4: modeling and optimization based on response surface methodology and artificial neural network. *J Mol Liq* **328**:115384 (2021).
24 Berends HM, Homburg T, Kunz I and Kurz P, K10 montmorillonite supported manganese catalysts for the oxidation of water to dioxygen. *Appl Clay Sci* **53**:174–180 (2011).
25 Xu H, Yan N, Qu Z, Liu W, Mei J, Huang W *et al*., Gaseous heterogeneous catalytic reactions over Mn-based oxides for environmental applications: a critical review. *Environ Sci Technol* **51**:8879–8892 (2017).
26 Lyu Y, Li C, Du X, Zhu Y, Zhang Y and Li S, Catalytic removal of toluene over manganese oxide-based catalysts: a review. *Environ Sci Pollut Res* **27**:2482–2501 (2020).
27 Mercier L and Detellier C, Intercalation of tetraalkylammonium cations into smectites and its application to internal surface-area measurements. *Clay Clay Miner* **42**:71–76 (1994).
28 Assemi S, Sharma S, Tadjiki S, Prisbrey K, Ranville J and Miller JD, Effect of surface charge and elemental composition on the swelling and delamination of montmorillonite nanoclays using sedimentation field-flow fractionation and mass spectroscopy. *Clay Clay Miner* **63**:457–468 (2015).
29 Tan X, Liu F, Hu L, Reed AH, Furukawa Y and Zhang G, Evaluation of the particle sizes of four clay minerals. *Appl Clay Sci* **135**:313–324 (2017).
30 Dolinská S, Schütz T, Znamenáčková I, Lovas M and Vaculíková L, Bentonite modification with manganese oxides and its characterization. *J Pol Miner Eng Soc* **16**:213–218 (2015).
31 Vaculíková L, Valovičová V, Plevová E, Napruszewska BD, Duraczyńska D, Karcz R *et al*., Synthesis, characterization and catalytic activity of cryptomelane/montmorillonite composites. *Appl Clay Sci* **202**:105977 (2021).
32 Krajisnik D, Dakovic M, Milojevic M, Malenovic A, Kragovic M, Bogdanovic DB *et al*., Properties of diclofenac sodium sorption onto natural zeolite modified with cetylpyridinium chloride. *Colloids Surf B* **83**:165–172 (2011).
33 Elzea JM, Odom IE and Miles WJ, Distinguishing well ordered opal-CT and opal-C from high temperature cristobalite by x-ray diffraction. *Anal Chim Acta* **286**:107–116 (1994).
34 Zhang Y, Wang M, Kang S, Pan T, Deng H, Shan W *et al*., Investigation of suitable precursors for manganese oxide catalysts in ethyl acetate oxidation. *J Environ Sci* **104**:17–26 (2021).
35 Ritz M, Vaculíková L, Kupková J, Plevová E and Bartoňová L, Different level of fluorescence in Raman spectra of montmorillonites. *Vib Spectrosc* **84**:7–15 (2016).
36 Potter RM and Rossman GR, The manganese(IV) oxides: identification, hydration and structural relationships by infrared spectroscopy. *Am Mineral* **64**:1199–1218 (1979).
37 Glerup M, Krumeich F, Nesper R, Fjellvåg H and Norby P, Microstructures and spectroscopic properties of cryptomelane-type manganese dioxide nanofibers. *J Phys Chem C* **112**:13134–13140 (2008).
38 Santos VP, Pereira MFR, Órfão JJM and Figueiredo JL, Synthesis and characterization of manganese oxide catalysts for the total oxidation of ethyl acetate. *Top Catal* **52**:470–481 (2009).
39 Tinsley DH and Sharp JH, Thermal analysis of manganese dioxide in controlled atmospheres. *J Therm Anal Calorim* **3**:43–48 (1971).
40 Klemm E, Wang J and Emig G, A comparative study of the sorption of benzene and phenol in silicalite. *Microporous Mesoporous Mater* **26**:11–21 (1998).

